JOURNAL OF THEORETICAL AND APPLIED MECHANICS
46, 3, pp. 597-620, Warsaw 2008

ON A NONLINEAR AND CHAOTIC NON-IDEAL VIBRATING SYSTEM WITH SHAPE MEMORY ALLOY (SMA)

Vinicius Piccirillo

UNESP – Sao Paulo State University, Department of Engineering Mechanics, Bauru, SP, Brazil e-mail: viniciuspiccirillo@yahoo.com.br

Jose Manoel Balthazar

UNESP – Sao Paulo State University, Department of Statistics, Applied Mathematical and Computation, Rio Claro, SP, Brazil; e-mail: jmbaltha@rc.unesp.br

Bento Rodrigues Pontes Jr.

UNESP – Sao Paulo State University, Department of Engineering Mechanics, Bauru, SP, Brazil e-mail: brpontes@feb.unesp.br

Jorge Luis Psalacios Felix

UNESP – Sao Paulo State University, Department of Statistics, Applied Mathematical and Computation, Rio Claro, SP, Brazil; e-mail: jorgelpfelix@yahoo.com.br

In this paper, we present nonlinear dynamic behaviour of a system which consists of a mass connected to a rigid support by a shape memory alloy (SMA) element and a damper. In order to disturb the system, a DC motor with limited power supply is connected to the mass, causing an interaction between the vibrating structure and the energy source. The SMA element is characterised using a one-dimensional phenomenological constitutive model, based on the classical Devonshire theory. We analyse the non-ideal system in form of two coupled nonlinear differential equations. Some interesting nonlinear phenomena as the Sommerfeld effect and nonlinear resonance including periodic, chaotic and hyperchaotic regime are presented.

Key words: shape memory, nonlinear dynamics, chaos, hiperchaos, Sommerfeld effect

1. Introduction

Intelligent and adaptive material systems and structures have become very important in engineering applications. The fundamental characteristic of these systems is the ability to adapt to environmental conditions. A new class of

materials with promising applications in structural and mechanical systems is the shape memory alloy (SMA). Mechanical behaviour of shape memory alloys, in particular, shows strong dependence on temperature.

Here, the focus is on certain aspects of shape memory alloy (SMA) actuators in smart structures, a task that goes beyond classical modelling approaches as it has to combine constitutive modelling with structural one in a highly interdisciplinary way.

Shape Memory Alloys (SMAs) consist of a group of metallic materials that demonstrate the ability to return to some previously defined shape or size when subjected to the appropriate thermal procedure. The SMAs appear in a low (usually martensite) and a high temperature phase (austenite). In literature, the shape memory effects (SMEs) are classified into the following three types: two-way effect, one-way effect and pseudoelasticity. The effects can appear in this sequence with increasing temperature. In the pseudoelastic effect, a SMA material achieves a very large strain upon loading that is fully recovered in a hysteresis loop upon unloading.

The shape memory effect occurs due to temperature and stress-dependent shift in the crystalline structure between two different phases called martensite and austenite. Martensite, the low temperature phase, is relatively soft whereas austenite, the high temperature phase, is relatively hard.

In the theoretical study by Bernardini and Vestroni (2003) a nonlinear dynamic non-isothermal response of pseudoelastic shape-memory oscillators was presented. Based on the work done by Bernardini and Vestroni (2003), Lacarbonara *et al.* (2004) studied a periodic and non-periodic thermomechanical response of a shape-memory oscillator and considered both isothermal and non-isothermal conditions under forced vibration.

In the recent work by Lagoudas *et al.* (2004) the authors presented numerically the response of a single-degree of freedom dynamic system having pseudoelastic SMA spring elements for damping and vibration isolation. Savi and Pacheco (2002) studied some characteristics of shape memory oscillators with one and two-degrees of freedom, showing the existence of chaos and hyperchaos through numerical simulations in such systems. Piccirillo *et al.* (2007a,b) presented a nonlinear dynamical characteristic of the thermomechanical response of the primary and secondary pseudoelastic oscillator where the method of multiple scales was used in order to obtain an approximate analytical solution.

We also remark that the study of non-ideal vibrating systems, that is, those where the excitation is influenced by the response of the system, is still

considered to be a major challenge in the theoretical and practical engineering research.

When the excitation is not influenced by the response, it is said to be an ideal excitation or an ideal source of energy. On the other hand, when the excitation is influenced by the response of the system, it is said to be non-ideal. Thus, depending on the excitation, one refers to vibrating systems as ideal or non-ideal.

This work concerns special kinds of problems called non-ideal problems. Non-ideal vibrating systems have two important properties: the jump phenomena and the increase in power required by the energy source operating near the resonance. This means that the steady state frequencies of the motor will usually increase as more power (voltage) is given to it in a step by-step fashion. When the resonance condition in the structure is reached, a greater part of this energy is consumed to generate large amplitude vibrations of the foundation without a sensible change in the motor frequency as before. If additional increase steps in voltage are made, one may reach a situation where the rotor will jump to higher rotation regimes, with no steady states being stable in between.

These above properties are known, in the current literature, as the Sommerfeld effect (Sommerfeld 1904). It was described in the classical book by Kononenko (1969), entirely devoted to this subject. A comprehensive and complete review of different approaches was given by Balthazar and Pontes (2005), Balthazar *et al.* (2003), Felix *et al.* (2005), Nayfeh and Mook (1979), Piccirillo *et al.* (2007c), without undeserving others authors.

Here we analyse the problem by taking a nonlinear SMA spring and a DC motor of limited power supply, exciting the considered dynamical system.

The goal of this paper is to analyse through numerical simulations the response of the proposed vibrating system and verify possible interactions between of the motor and vibrating structure.

2. Modelling of the system

We consider an electric motor operating on a structure. Figure 1 shows the model of such a system to be investigated in this paper. The vibrating system consists of a mass M, SMA element and linear damping element with the viscous damping coefficient c. On the object with the mass M, a non-ideal DC motor is placed, with the driving rotor having the moment of inertia J. r is the eccentricity of the unbalanced mass (Fig. 1b).

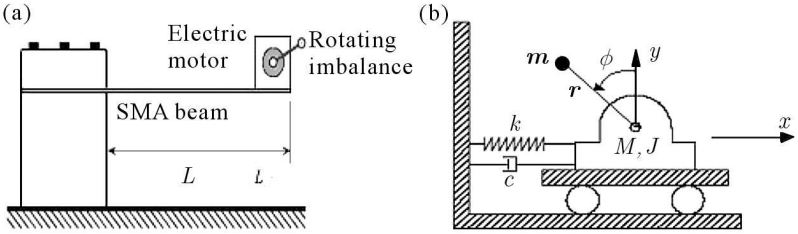

Fig. 1. (a) Physical model, (b) mathematical model with limited power supply

The shape memory behaviour is described by a polynomial constitutive model (Falk, 1980). This is a one-dimensional model which represents the shape memory and pseudoelastic effects considering polynomial free energy that depends on temperature and one-dimensional strain E. Therefore, the restoring force of the oscillator is given by

$$K = K(x,T) = \overline{q}(T - T_M)x - \overline{b}x^3 + \overline{e}x^5 \tag{2.1}$$

where

$$\overline{q} = \frac{qA}{L}\overline{b} = \frac{bA}{L^3}\overline{e} = \frac{eA}{L^5} \tag{2.2}$$

The parameters $\overline{q}$, $\overline{b}$ and $\overline{e}$ are positive constants, while T_M is the temperature below which the martensitic phase is stable. The variable x represents the displacement associated with the SMA element.

We will denote by ϕ the angular displacement of the rotor.

The total kinetic K_E and potential P_E energies of the coupled system and the non-conservatives forces G and torque Γ are given by

$$\begin{aligned} K_E &= \frac{1}{2}M\dot{x}^2 + \frac{1}{2}J\dot{\phi}^2 + \frac{1}{2}(\dot{x} - r\dot{\phi}\cos\phi)^2 + \frac{1}{2}m(r\dot{\phi}\sin\phi)^2 \\ P_E &= \frac{1}{2}\overline{q}(T - T_M)x^2 - \frac{1}{4}\overline{b}x^4 + \frac{1}{6}\overline{e}x^6 \\ G &= c\dot{x} \qquad\qquad \Gamma(\dot{\phi}) = S(\dot{\phi}) - H(\dot{\phi}) \end{aligned} \tag{2.3}$$

where $S(\dot{\phi})$ is the controlled torque of the unbalanced rotor and $H(\dot{\phi})$ is the resistant torque of the unbalanced rotor.

Thus, we will obtain the following Lagrange's equations of motion

$$\begin{aligned} &(M+m)\ddot{x} + c\dot{x} - mr(\ddot{\phi}\cos\phi - \dot{\phi}^2\sin\phi) + \overline{q}(T - T_M)x - \overline{b}x^3 + \overline{e}x^5 = 0 \\ &(J + mr^2)\ddot{\phi} - mr\ddot{x}\cos\phi = \Gamma(\dot{\phi}) \end{aligned} \tag{2.4}$$

It is convenient to proceed with a dimensionless position and time, according to

$$u = \frac{x}{L} \qquad \tau = \omega_0 t \tag{2.5}$$

in such a way that Eq. (2.4) is rewritten in the following form

$$\begin{aligned} &\ddot{u} + 2\mu\dot{u} + (\theta - 1)u - \alpha u^3 + \gamma u^5 - \lambda(\ddot{\phi}\cos\phi - \dot{\phi}^2 \sin\phi) = 0 \\ &\ddot{\phi} - \eta\ddot{u}\cos\phi = \xi_1 - \xi_2\dot{\phi} \end{aligned} \tag{2.6}$$

where the dot represents time differentiation, and the dimensionless variables are given by

$$\begin{aligned} &\omega_0^2 = \frac{qAT_M}{(M+m)L} \qquad \alpha = \frac{bA}{(M+m)L\omega_0^2} \qquad \theta = \frac{T}{T_M} \\ &\mu = \frac{c}{2(M+m)\omega_0} \qquad \gamma = \frac{eA}{(M+m)L\omega_0^2} \qquad \lambda = \frac{mr}{(M+m)L} \\ &\eta = \frac{mrL}{(J+mr^2)} \end{aligned} \tag{2.7}$$

Characteristic curves of the energy source (DC motor) are assumed to be straight lines

$$\Gamma = \xi_1 - \xi_2\dot{\phi} \tag{2.8}$$

Note that the parameter ξ_1 is related to the voltage of the considered DC motor and ξ_2 is a constant for each of the considered motors (Warmiński *et al.*, 2001). The voltage is a possible control parameter for the problem.

3. Numerical simulation

The objective of this section is to analyse the vibrating problem defined by Fig. 1, taking into account the linear torque defined by equation (3.1). Numerical simulations were carried out by using the Matlab-Simulink®. In all numerical simulations, to analyse the behaviour of the non-ideal dynamical system, the spring was assumed to be made of a (Cu-Zn-Al-Ni) alloy with properties presented in Table 1.

Table 1. Material constants for Cu-Zn-Al-Ni alloy (Savi *et al.*, 2002)

q [MPa/K]	b [MPa]	e [MPa]	T_M [K]	T_A [K]
523.29	$1.868 \cdot 10^7$	$2.186 \cdot 10^9$	288	364.3

Putting down Eq. (2.6) into state variables, we obtain

$$\begin{aligned}
&\dot{u}_1 = u_2 \qquad\qquad \dot{u}_3 = u_4 \\
&\dot{u}_2 = \frac{1}{1-\lambda\eta\cos^2 u_3}\cdot \\
&\quad \cdot\Big\{\lambda[(\xi_1 - \xi_2 u_4)\cos u_3 - u_4^2 \sin u_3] + \alpha u_1^3 - \gamma u_1^5 - (\theta-1)u_1 - 2\mu u_2\Big\} \\
&\dot{u}_4 = \frac{\xi_1}{1-\lambda\eta\cos^2 u_3} + \\
&\quad + \frac{\eta\cos u_3}{1-\lambda\eta\cos^2 u_3}\Big[\alpha u_1^3 - \gamma u_1^5 - (\theta-1)u_1 - 2\mu u_2 - \frac{\xi_2 u_4}{\eta\cos u_3} - \lambda u_4^2 \sin u_3\Big]
\end{aligned} \tag{3.1}$$

Furthermore, in all numerical simulations, we considered the parameters: $\mu = 0.01$, $\eta = 0.6$, $\lambda = 0.4$ and $\xi_2 = 1.5$. Note that the passage through the resonance is obtained by varying the angular velocity $\dot{\phi}$ of the DC motor.

In order to illustrate the response of the non-ideal system, we consider a temperature where the martensitic phase is stable ($\theta = 0.7$). In the second situation, we examine an intermediate temperature where the martensitic and austenitic phases are both present in the alloy ($\theta = 1.03$), and we analyse the response at higher temperatures ($\theta = 2$) when the alloy is fully austenitic. We also plot the Poincaré section which represents a surface of the section $(x_1(\tau_n), x_2(\tau_n))$. The points $(x_1(\tau_n), x_2(\tau_n))$ are captured for $\tau_n = nT$, where $n = 1, 2, 3, \ldots$, with the period $T = 2\pi/\Omega_M$ (Zukovic and Cveticanin, 2007). The average angular velocity Ω_M is obtained numerically

$$\Omega_M = \frac{\phi(\tau_1) - \phi(0)}{\tau_1} = \frac{u_3(\tau_1) - u_3(0)}{\tau_1} \tag{3.2}$$

where τ_1 is a long time period for numerical calculation.

The greatest interaction between the vibrating system and the energy source occurs at the resonance. We define the resonance region as

$$\frac{d\varphi}{dt} - \omega = O(\varepsilon) \tag{3.3}$$

where $d\varphi/dt$ is the angular velocity, ε is the small parameter of the order of 10^{-3}, ω – natural frequency of the system.

Generally, for a wide range of physical parameters, when the system was started off, the angular velocity of the rotor increases until it reaches the neighbourhood of the natural frequency ω. Then, depending upon physical parameters, values of $d\varphi/dt$ increase beyond the resonance region (pass through) or remains close to ω (capture).

3.1. Martensitic phase

In this section, we study the problem of a vibrating system depicted in Fig. 1, taking into account temperature $\theta = 0.7$, where the martensitic phase is stable.

It is known that dynamics of a system close to the fundamental resonance region may be analysed through a frequency-response diagram, which is obtained by plotting the amplitude of the oscillating system versus the frequency of the excitation term. For the non-ideal system, this graph is estimated by numerical simulation defining the amplitude as the maximum absolute value of the amplitude of oscillation, and the frequency as the mean value of the rotational speed of the motor (Belato *et al.*, 2001).

In Fig. 2, the amplitude of motion is plotted as function of $\dot{\phi}$. As expected, we observe the occurrence of the Sommerfeld effect. In vibrating nonlinear systems, the Sommerfeld effect is an important irregular sink of irregular vibrations (Tsuchida *et al.*, 2005). The curves were obtained by allowing the system to achieve steady-state motion, while the control parameter was fixed. Then, the amplitude of the steady-state response was measured. The curve was calculated, using an increment $\Delta\xi_1 = 0.1$, as the variation of the control parameter ξ_1 in the interval $[0, 3.1]$ and holding in the new position until a new steady state was achieved. The circle symbols represent the steady state solutions. Figure 2a shows the results for increasing ξ_1, while Fig. 2b shows the results for decreasing ξ_1.

For the chosen parameter, we may note that the jump phenomena occur in different forms, when the motor frequency is increased or decreased, where there is a discontinuous jump. This jump appears on the frequency response curve as a discontinuity which indicates a region where steady-state conditions do not exist. This resonance curve has an untypical shape.

In Fig. 2a, the solution exhibits more complicated and different behaviour confirmed by the presence of three jumps in the graph. The first jump occurs between the points A and B. In the first case, the velocity of the rotor passes through the superharmonic resonance of the motor frequency for $0 < \dot{\phi} \leqslant 0.14$. As ξ_1 increases, the secondary jump from the point C to D takes place. In this case, the velocity of the rotor passes through the subharmonic resonance for

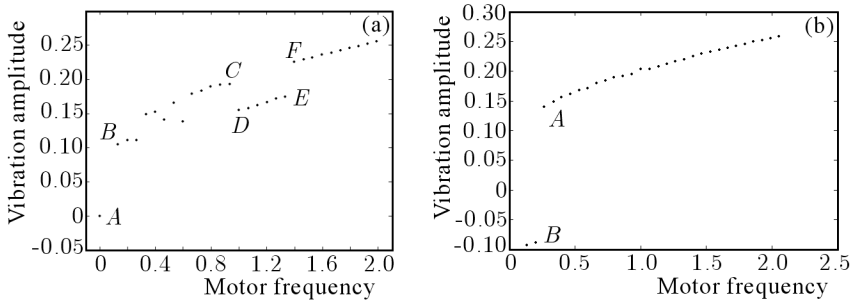

Fig. 2. Frequency-response curves for the non-ideal system for $\theta = 0.7$: (a) for increasing ξ_1, (b) for decreasing ξ_1

$0.92 \leqslant \dot{\phi} \leqslant 1.02$. As ξ_1 increases, the amplitude slowly increases through the point D to E. As ξ_1 increases further, a jump takes place from the point E to F. In this case, the velocity of the rotor passes through the subharmonic resonance for $1.32 \leqslant \dot{\phi} \leqslant 1.4$. These jumps cause an increase in the amplitude of motion. In Fig. 2b the amplitude decreases slowly as the control parameter is reduced, a jump from the point A to B takes place. In this case, the velocity of the rotor passes through the superharmonic resonance for $0.2 < \dot{\phi} < 0.28$.

The Lyapunov exponent may be used to measure the sensitive dependence upon initial conditions. It is an index for chaotic behaviour. Different solutions of a dynamical system, such as fixed points, periodic motions, quasiperiodic motion and chaotic motion can be distinguished by it. If two chaotic trajectories start close one to another in the phase space, they will move exponentially away from each other for short times on the average.

We evaluate the Lyapunov exponents using the classical method described in Wolf *et al.* (1985). The main formula is

$$\lambda = \frac{1}{tN} \sum_{i=1}^{N} \ln \frac{d_i(t)}{d_i(0)} \tag{3.4}$$

where λ denotes the Lyapunov exponents, the index i corresponding initial positions, and d is the separation between two close trajectories.

Assume that λ_i $(i = 1, 2, 3, 4)$ are the Lyapunov exponents of system (2.6), satisfying the condition $\lambda_1 \geqslant \lambda_2 \geqslant \lambda_3 \geqslant \lambda_4$. The dynamical behaviours of system (2.6) can be classified as follows based on the Lyapunov exponents:
— the non-ideal system has a chaotic attractor

$$\lambda_1 > 0 \qquad \lambda_2 = 0 \qquad \lambda_3 < 0 \qquad \lambda_4 < 0$$

— the non-ideal system has a periodic attractor

$$\lambda_1 = 0 \qquad \lambda_2 < 0 \qquad \lambda_3 < 0 \qquad \lambda_4 < 0$$

— the non-ideal system is hyperchaotic

$$\lambda_1 > 0 \qquad \lambda_2 > 0 \qquad \lambda_3 < 0 \qquad \lambda_4 < 0$$

in all simulations, we consider that: λ_1, λ_2, λ_3 and λ_4.

The Lyapunov exponents of the solution to the non-ideal dynamical system, Eq. (2.6), are plotted in Fig. 3 for ξ_1 ranging form 0.1 to 2.

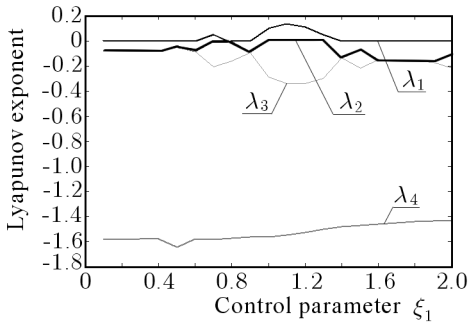

Fig. 3. Lyapunov exponent versus control parameter

Through Fig. 3, we can build Table 2 that shows types of attractors of system (2.6), which are encountered as the parameter ξ_1 is varied in the range $0.1 \leqslant \xi_1 \leqslant 2$ and $\theta = 0.7$.

Table 2. Attractor types for $\theta = 0.7$

Control parameter (ξ_1)	θ	Attractor type
0.1 – 0.67	0.7	periodic
0.68 – 0.78	0.7	chaotic
0.79 – 0.98	0.7	periodic
0.99 – 1.32	0.7	hyperchaotic
1.33 – 2.00	0.7	periodic

In order to complete the dynamic analysis of the problem, a number of numerical simulations are done for various control parameters ξ_1.

When ξ_1 is varied in the intervals $0.1 \leqslant \xi_1 \leqslant 0.67$, $0.79 \leqslant \xi_1 \leqslant 0.98$ and $1.33 \leqslant \xi_1 \leqslant 2$ we observe that the considered non-ideal system vibrates periodically. For example, Fig. 4 illustrates the case when the angular velocity is captured into the resonance region for $\xi_1 = 0.8218$. The nature of motion is confirmed in Fig. 4c through the power spectrum.

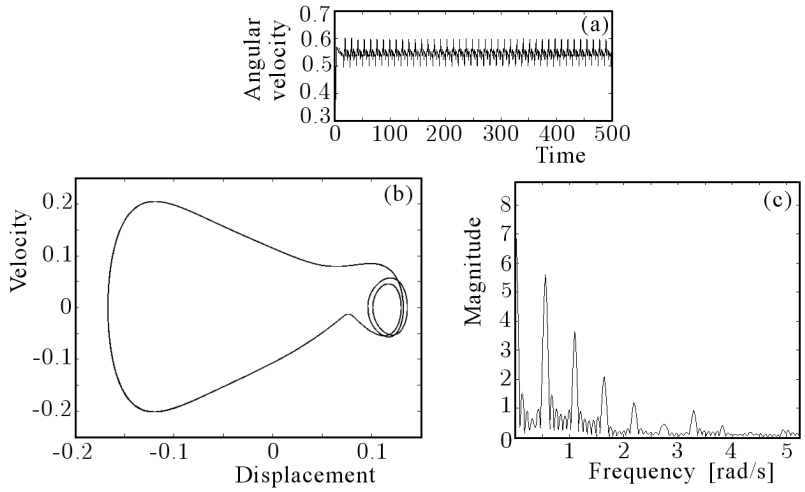

Fig. 4. (a) Angular velocity time response, (b) phase portrait and (c) power spectrum for $\xi_1 = 0.8218$ and $\theta = 0.7$

In the next case, to obtain a chaotic regime in the interval $0.68 \leqslant \xi_1 \leqslant 0.78$, we assumed $\xi_1 = 0.7$. Solving numerically system (2.6), we obtain Fig. 5. A strange attractor on the Poincaré section (see Fig. 5d) obtained for the

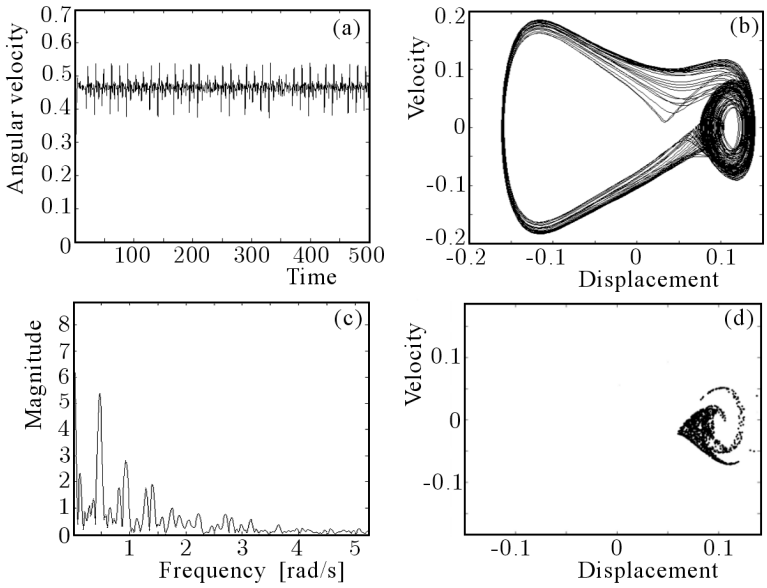

Fig. 5. (a) Angular velocity time response, (b) phase portrait, (c) power spectrum and (d) Poincaré section for $\xi_1 = 0.7$ and $\theta = 0.7$

non-ideal system has a complicated fractal structure with features chaotic motion. Positive sign of the maximal Lyapunov exponents in Fig. 3, for $\theta = 0.7$, confirms that the system vibrates chaotically. In this case, the angular velocity of the rotor is below the resonance region.

For the parameter values mentioned in the previous section and the control parameter $\xi_1 = 1$, the phase trajectory and Poincaré's section are plotted in Fig. 6. The existence of the strange attractor signifies hyperchaotic motion, which is evident because two Lyapunov exponents are positive. Furthermore, we observe that the angular velocity of the rotor is above the resonance region.

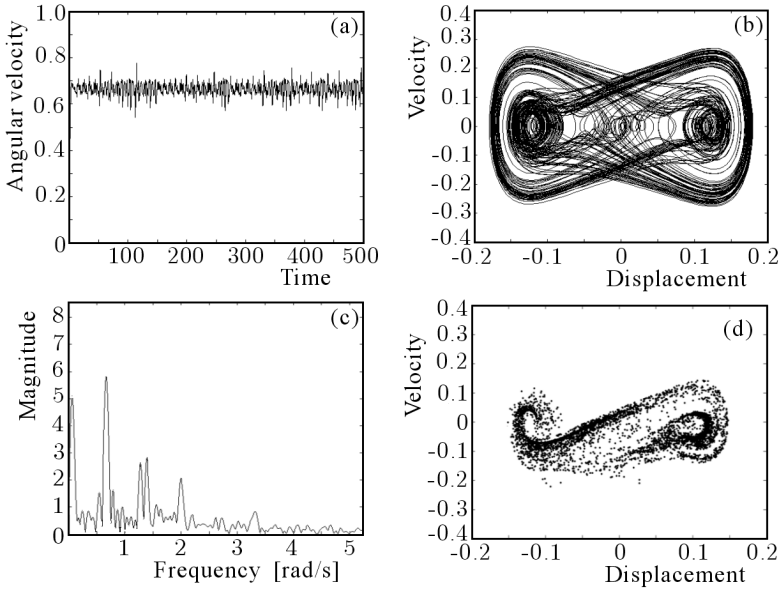

Fig. 6. (a) Angular velocity time response, (b) phase portrait, (c) power spectrum and (d) Poincaré section for $\xi_1 = 1$ and $\theta = 0.7$

3.2. Martensitic and austenitic phases

The cases where the shape memory elements have intermediate temperatures, i.e., both martensitic and austenitic phases are stable $\theta = 1.03$ is now considered.

Figure 7 shows the presence of the Sommerfeld effect during the passage through the resonance region by varying the control parameter ξ_1 in the interval $0.1 \leqslant \xi_1 \leqslant 0.7$. The curve was calculated using an increment $\Delta\xi_1 = 0.02$ as the variation of the control parameter. The circle symbols represent steady

state solutions. Figure 7a shows the results for increasing ξ_1, while Fig. 7b shows the results for decreasing ξ_1.

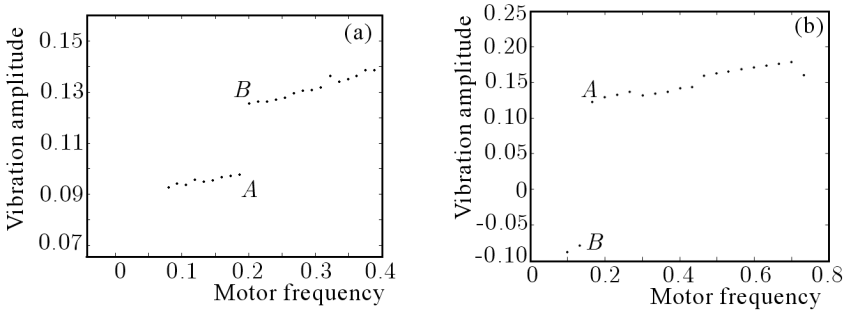

Fig. 7. Frequency-response curves for the non-ideal system for $\theta = 1.03$: (a) for increasing ξ_1, (b) for decreasing ξ_1

In Fig. 7a it is seen that when the control parameter ξ_1 is gradually increased, the motor frequency is increased slowly and the amplitude of motion slowly increases until the point A is reached. As ξ_1 is increased further, a jump from the point A to point B takes place with accompanying increment in the amplitude. In this case, the velocity of the rotor passes through the resonance region for $0.18 < \dot{\phi} < 0.2$. The experiment is started at a frequency corresponding to the control parameter $\xi_1 = 0.7$ on the curve in Fig. 7b. As the motor frequency is reduced, the amplitude of motion decreased slowly to the point A. As the motor frequency is decreased further, a jump form the point A to point B takes place, with accompanying decrement in the amplitude of motion, in this case, the velocity of the rotor passes through the resonance region for $0.13 < \dot{\phi} < 0.17$.

As in the previous section, the Lyapunov exponent of the system is computed and its connection with the control parameter ξ_1 is shown in Fig. 8. The results show that there appears a positive exponent, which is an indicator of chaotic dynamics.

Here, the Lyapunov exponent of the non-ideal system is listed in Table 3 for different values of ξ_1.

Several aspects of nonlinear dynamic behaviour of the system were discussed in previous sections. They show that the non-ideal system exhibits both regular and chaotic motion.

In order to illustrate the nonlinear response of the non-ideal system with shape memory elements for $\theta = 1.03$, different control parameters are considered.

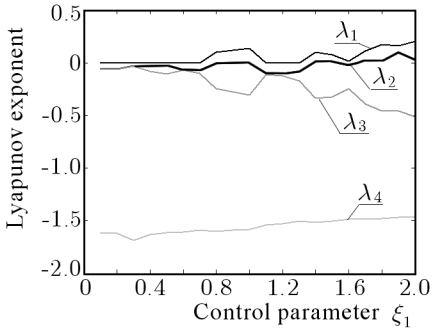

Fig. 8. Lyapunov exponent versus control parameter

Table 3. Attractor type for $\theta = 1.03$

Control parameter (ξ_1)	θ	Attractor type
0.1 – 0.74	1.03	periodic
0.75 – 1.06	1.03	chaotic
1.07 – 1.3	1.03	periodic
1.31 – 1.39	1.03	chaotic
1.4 – 1.59	1.03	hyperchaotic
1.6 – 1.69	1.03	chaotic
1.7 – 2.00	1.03	hyperchaotic

When ξ_1 is varied in the intervals $0.1 \leqslant \xi_1 \leqslant 0.74$ and $1.07 \leqslant \xi_1 \leqslant 1.3$, we observe that the considered non-ideal system vibrates in periodically. If $\xi_1 = 1.2$, the results are shown in Fig. 9. In this case, we observe that the angular velocity of the rotor is above the resonance region.

The chaotic attractor of the non-ideal system is obtained in the intervals $0.75 \leqslant \xi_1 \leqslant 1.06$, $1.31 \leqslant \xi_1 \leqslant 1.39$ and $1.6 \leqslant \xi_1 \leqslant 1.69$. This behaviour of the non-ideal system with the parameter $\xi_1 = 0.75$ is shown in Fig. 10. Figure 10a illustrates that the angular velocity of the rotor is above the resonance region. In Fig. 10c, a broadband character observed in the power spectrum is characteristic for the chaotic solution. Here, we use the Poincaré section to characterise the dynamics of the system. In Fig. 10d a strange attractor of the system for $\xi_1 = 0.75$ and $\theta = 1.03$ is presented.

When we consider the intervals $1.4 \leqslant \xi_1 \leqslant 1.59$ and $1.7 \leqslant \xi_1 \leqslant 2$, it is possible to observe that the response becomes hyperchaotic (see Table 2). In order to illustrate this behaviour, the system with $\xi_1 = 1.7$ is considered. Figure 11a presents the response of the system where the angular velocity is above the resonance region. In Figs. 11b,c,d the phase portraits and Poincaré

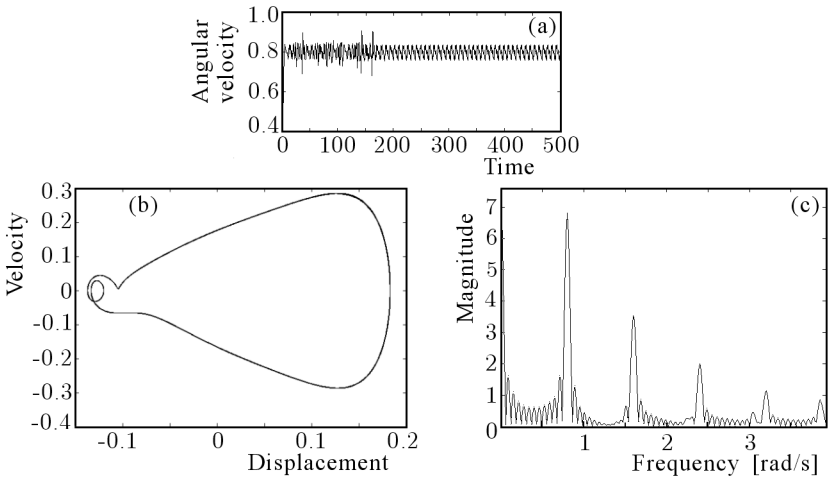

Fig. 9. (a) Angular velocity time response, (b) phase portrait and (c) power spectrum for $\xi_1 = 1.2$ and $\theta = 1.03$

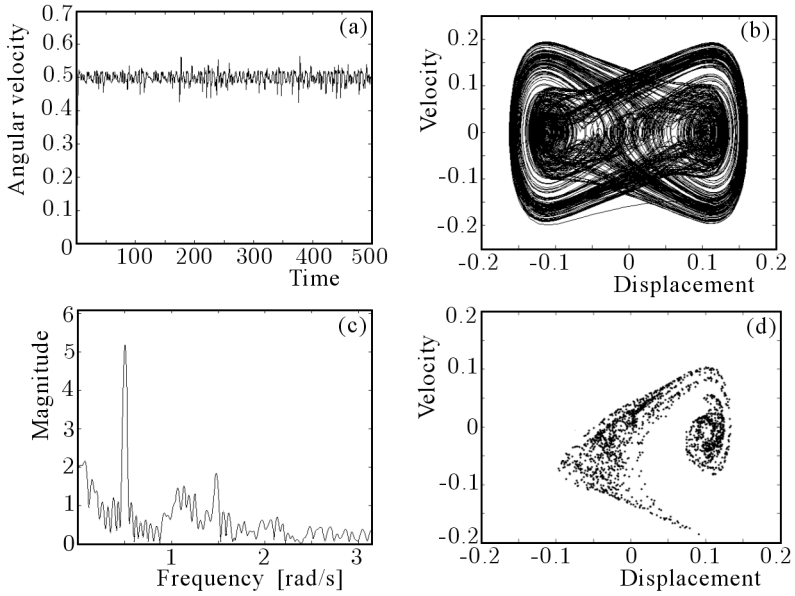

Fig. 10. (a) Angular velocity time response, (b) phase portrait, (c) power spectrum and (d) Poincaré section for $\xi_1 = 0.75$ and $\theta = 1.03$

sections related to this motion are shown. The strange attractor appears on the phase space, indicating hyperchaotic motion. The existence of two positive Lyapunov exponents assures this behaviour.

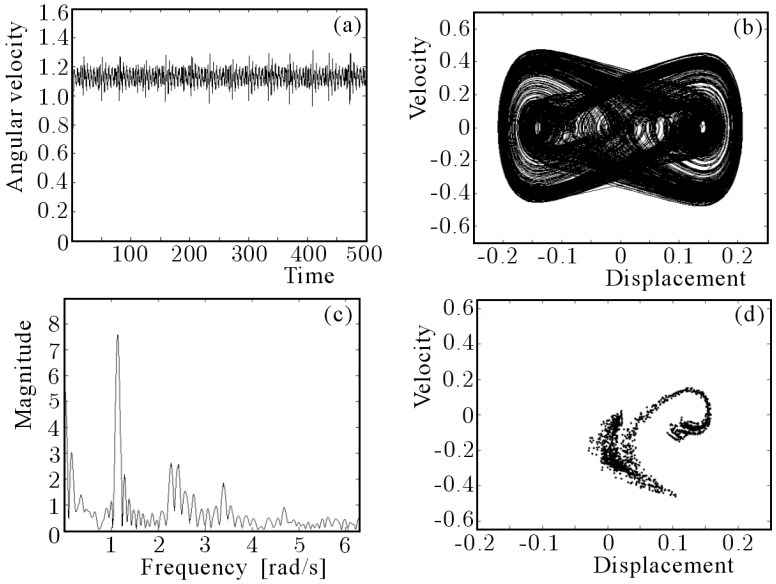

Fig. 11. (a) Angular velocity time response, (b) phase portrait, (c) power spectrum and (d) Poincaré section for $\xi_1 = 1.7$ and $\theta = 1.03$

3.3. Austenitic phase

Now, higher temperature is considered and the austenitic phase is stable ($\theta = 2$). In Fig. 12 the presence of the Sommerfeld effect during the passage through the resonance region by varying the control parameter ξ_1 in the interval $0.1 \leqslant \xi_1 \leqslant 2$ is shown. The curve was calculated using an increment $\Delta\xi_1 = 0.1$ as the variation of the control parameter. The circle symbols represent steady state solutions. Figure 12a shows the results for increasing ξ_1, while Fig. 12b shows the results for decreasing ξ_1.

For the chosen parameter ($\theta = 2$), no change in the curve shape, except a near jump region when the mean frequency $\dot{\phi}$ is increased or decreased, was observed.

Suppose that the experiment is started at $\xi_1 = 0.1$ in Fig. 12a. As ξ_1 is increased, the amplitude of motion increases until the point A is reached. As ξ_1 is increased further, a jump takes place from the point A to point B, with accompanying increment in the amplitude of motion, after which the

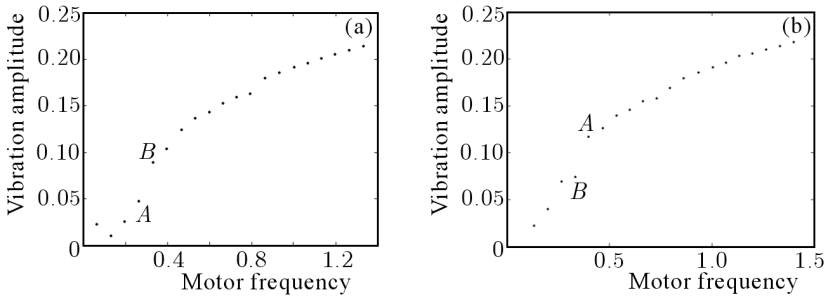

Fig. 12. Frequency-response curves for the non-ideal system for $\theta = 2$: (a) for increasing ξ_1, (b) for decreasing ξ_1

amplitude of motion increases with ξ_1. In this case, the velocity of the rotor passes through the resonance region for $0.26 < \dot{\phi} < 0.34$.

If the process is reversed, the amplitude of motion decreases as the motor angular velocity decreases until the point A is reached. As motor frequency is decreased further, a jump from the point A to point B takes place with accompanying decrementnt in the amplitude of motion, after which the amplitude of motion decreases slowly with decreasing motor frequency. In this case, the velocity of the rotor passes through the resonance region for $0.32 < \dot{\phi} < 0.4$.

To characterise irregular chaotic response forms creating a transition zone between one and another type of regular steady resonant motion, a Lyapunov exponent diagram is constructed. Figure 13 shows the dynamics of the Lyapunov exponents for $\theta = 2$, where, in this case, the Lyapunov exponents are positive, negative or null, depending of the control parameter.

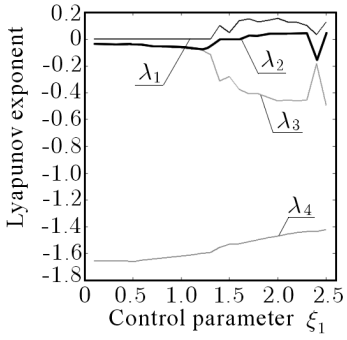

Fig. 13. Lyapunov exponent versus control parameter

Based on Fig. 13, Table 4 is built. Negative Lyapunov exponent in Fig. 13 confirms that the system vibrates periodically in the interval $0.1 \leqslant \xi_1 \leqslant 1.31$.

Positive Lyapunov exponent in Fig. 13 confirms that the system vibrates chaotically in the intervals $1.32 \leqslant \xi_1 \leqslant 1.6$ and $2.31 \leqslant \xi_1 \leqslant 2.4$. In the case where two Lyapunov exponents are positive, the system vibrates hyperchaotically.

Table 4. Attractor type for $\theta = 2$

Control parameter (ξ_1)	θ	Attractor type
0.1 – 1.31	2	periodic
1.32 – 1.6	2	chaotic
1.61 – 2.3	2	hyperchaotic
2.31 – 2.4	2	chaotic
2.41 – 2.5	2	hyperchaotic

Figure 14 shows interesting dynamical behaviour for $\theta = 2$ and $\xi_1 = 1$. We observe that the angular velocity of the rotor is below the resonance region. In this case, the motion is periodic.

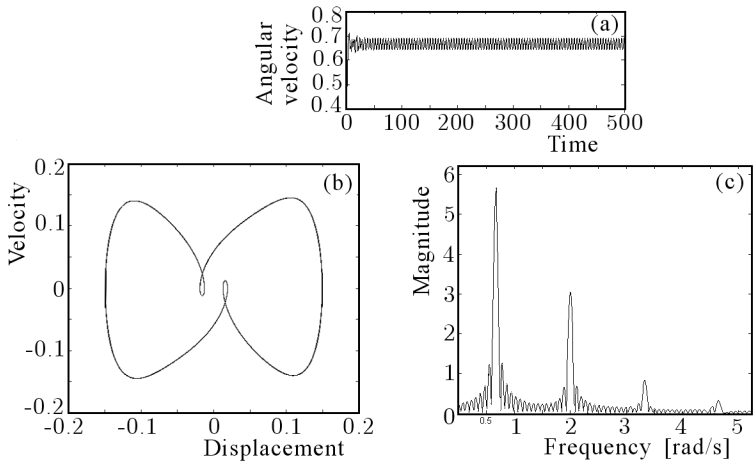

Fig. 14. (a) Angular velocity time response, (b) phase portrait, (c) power spectrum for $\xi_1 = 1$ and $\theta = 2$

Figure 15 shows another kind of behaviour, for $\xi_1 = 1.5$ and $\theta = 2$. We observe that when the angular velocity of the rotor is captured in the resonance region, chaos is found.

Figure 16 shows interesting dynamical behaviour. For $\xi_1 = 2$ and $\theta = 2$, we observe that the angular velocity of the rotor is above the resonance region. Here, we have two positive Lyapunov exponents, meaning that there is hyperchaos.

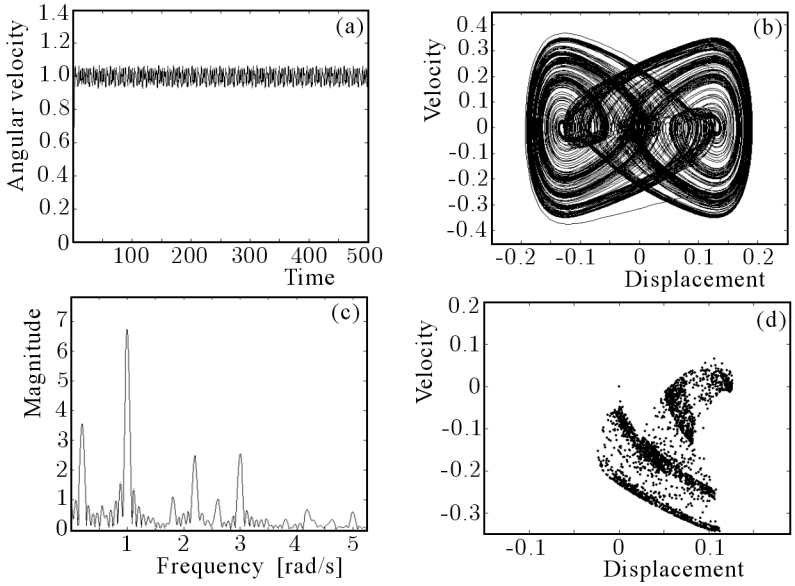

Fig. 15. (a) Angular velocity time response, (b) phase portrait, (c) power spectrum and (d) Poincaré section for $\xi_1 = 1.5$ and $\theta = 2$

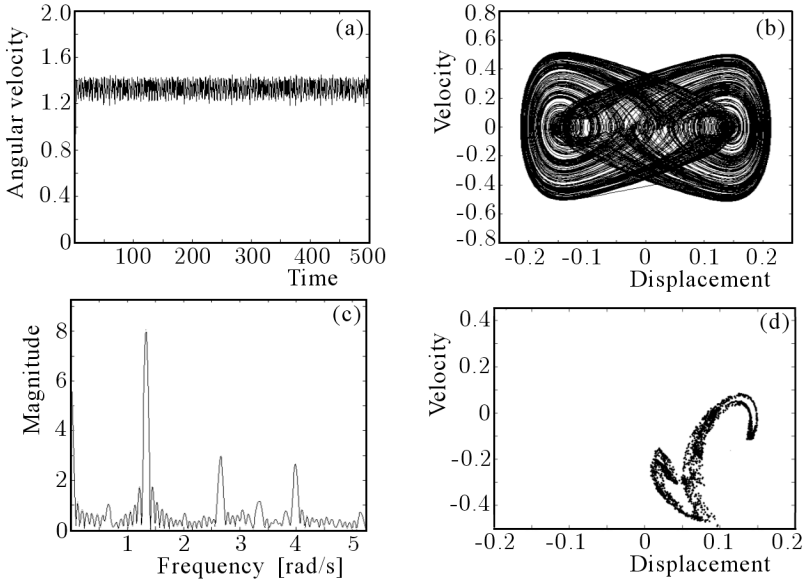

Fig. 16. (a) Angular velocity time response, (b) phase portrait, (c) power spectrum and (d) Poincaré section for $\xi_1 = 2$ and $\theta = 2$

3.4. Influence of temperature on system response

In the design of (SMA) vibrating systems, temperature is of great importance. It was noticed that in such systems, the control parameter ξ_1 (related to voltage of the DC motor) and temperature, have strong influence on the system response. Now, we present results found by variation of temperature with the control parameter dept constant.

In this section, the numerical results are plotted to illustrate the influence of temperature on the dynamical behaviour of the system. In order to illustrate this problem a simulation where temperature varies between two levels, as indicated in Fig. 17, is presented.

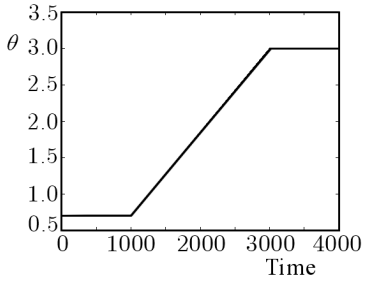

Fig. 17. Temperature history

In Fig. 17, we notice that for the time interval $0 \leqslant \tau \leqslant 1000$ the system has $\theta = 0.7$. In this interval the martensitic phase is stable. From $\tau = 1000$ the system starts to exhibit gradually increasing temperature. In the interval $1000 < \tau < 1266$, the system still remains with the martensitic phase stable, however it has $\theta \in [0.7, 1]$, but for $\tau = 1266$ the martensitic phase transformation (martensitic for austenitic) in the interval $1266 \leqslant \tau \leqslant 1493$ begins. From $\tau > 1493$, the alloy becomes fully austenitic and $\theta \in [1.26, 2.9]$ with $1493 < \tau < 3000$. For $3000 \leqslant \tau \leqslant 4000$ it has $\theta = 3$.

Considering the value of $\xi_1 = 0.7$ and variation of temperature in Fig. 17, we obtain a new representation of the time history in this situation, Fig. 18.

Figure 19a shows the angular velocity of the motor. Figure 19b shows the dynamical response, and Fig. 19c shows the phase diagram.

Notice (see Fig. 19) that there occurs a decrease as much in the velocity as in the displacement of the system. The source of the distinctive mechanical behaviour of these materials is a crystalline phase transformation between low symmetry and a less ordered product phase (martensite) that occurs between $\theta \in [0.7, 1]$. In this case, the behaviour of the system is irregular, but when the phase transformation occurs for high symmetry, the highly ordered parent

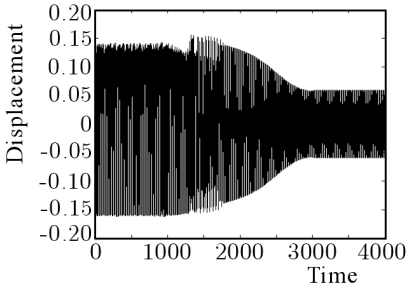

Fig. 18. Time history for $\xi_1 = 0.7$

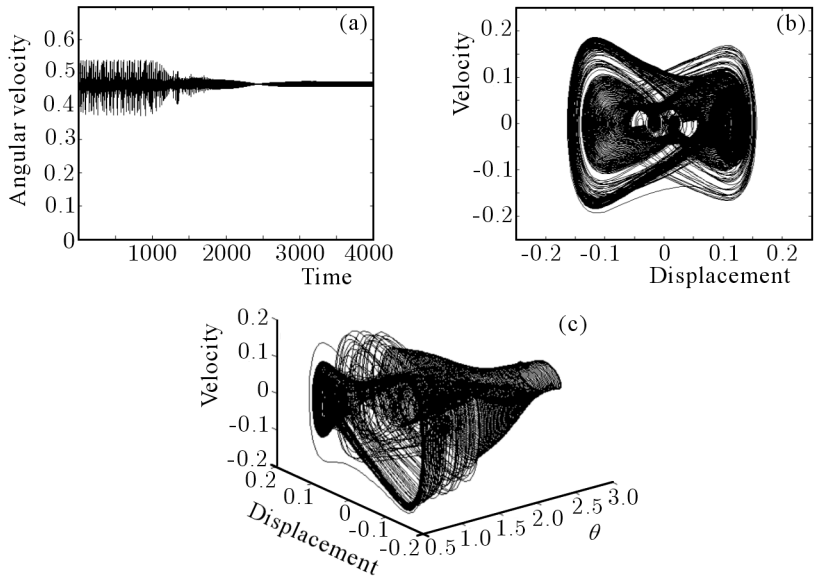

Fig. 19. (a) Angular velocity of the motor, (b) phase portrait and (c) phase diagram for $\xi_1 = 0.7$ and $\theta \in [0.7, 3]$

phase (austenite) for $\theta \in [1.26, 3]$ appears and the behaviour of the system is then regular.

Figure 20 shows the Lyapunov exponent for variation of the parameter θ, making noticeable the moment when the motion becomes chaotic.

By comparing the Fig. 19 and Fig. 20, notice that for $\theta = 0.7$ and $0 \leqslant \tau \leqslant 1000$ the angular velocity is below the resonance region and the dynamical behaviour is chaotic because a positive Lyapunov exponent exists. With

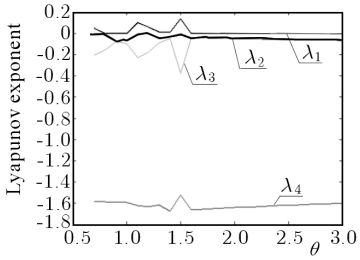

Fig. 20. Lyapunov exponent for $\xi_1 = 0.7$

the increase of the temperature between $0.7 \leqslant \theta \leqslant 1$ and $1000 < \tau < 1266$, the angular velocity continually decreases below the resonance region, however the dynamics of the system drastically changes and becomes periodic, which is reflected by the Lyapunov exponent (see Fig. 20), which changes its sign from positive to negative near $\theta = 0.8$. As θ is increased further, the martensitic phase transformation happens (martensitic to austenitic) in the interval $1 < \theta \leqslant 1.26$ and $1266 < \tau \leqslant 1493$. In this situation the angular velocity is captured by the resonance region between $1.21 < \theta \leqslant 1.24$ and motion of the system comes back to chaos. In the interval $1.26 < \theta \leqslant 1.59$ with the angular velocity outside the resonance region, the system continues having chaotic behaviour (a positive Lyapunov exponent exists) and, finally, for $1.6 \leqslant \theta \leqslant 3$, the Lyapunov exponent abruptly changes the sign to negative and the behaviour of the system becomes periodic.

4. Conclusion

In this paper, we analysed the influence of SMA spring on an non-ideal system during the passage through the resonance. The torque generated by a DC motor is limited and, according to the classical Kononenko theory, assumed as a straight line. An important characteristic of such systems is the temperature dependence, which changes the dynamical behaviour according to each phase of SMA.

The analysis is developed by considering different temperature sets for the shape memory element. Depending on the parameter configuration, the system displays various dynamical responses.

During the passage through the resonance of the motor-structure system, which is modelled as a SMA oscillator with an non-ideal excitation, "severe" vibrations appear. Poincaré sections, Lyapunov exponents and phase por-

traits have been used to examine the system dynamics. The interaction between the motor and the oscillating system is evidenced in different phase portraits.

The numerical results presented, in this paper show that it is possible to get regular, chaotic and hyperchaotic motion depending on the control parameter ξ_1. The Lyapunov exponents have been calculated in order to characterise chaotic and hyperchaotic orbits. The model displays the occurence of the expected Sommerfeld effect of getting stuck at resonance and jump phenomena.

Acknowledgement
The authors thank CAPES, FAPESP and CNPq for financial support.

References

1. Balthazar J.M., Mook D.T., Weber H.I., Reyolando M.L.R.F., Fenili A., Belato D., Felix J.L.P., 2003, An overview on non-ideal vibrations, *Meccanica*, **38**, 613-621

2. Balthazar J.M., Pontes Jr. B.R., 2005, On friction induced nonlinear vibrations: A source of fatigue, *Damage Prognosis – For Aerospace, Civil and Mechanical System*, Edited by D. Inman, John Wiley and Sons

3. Belato D., Weber H.I., Balthazar J.M., Mook D.T., 2001, Chaotic vibrations of a non-ideal electro-mechanical system, *International Journal of Solids and Structures*, **38**, 1699-1706

4. Bernardini D., Vestroni F., 2003, Non-isothermal oscillations of pseudoelastic devices, *International Journal of Non-Linear Mechanics*, **38**, 1297-1313

5. Falk F., 1980, Model free – energy, mechanics and thermodynamics of shape memory alloys, *ACTA Metallurgica*, **12**, 1773-1780

6. Felix J.L.P., Balthazar J.M., Brasil R.M.F.L.R.F., 2005, On tuned liquid column dampers mounted on a structural frame under a non-ideal excitation, *Journal of Sound and Vibration*, **282**, 1285-1292

7. Konokenko V.O., 1969, *Vibrating Problems With a Limited Power Supply*, Illife, London

8. Lacarbonara W., Bernardini D., Vestroni F., 2004, Nonlinear thermomechanical oscillations of shape memory devices, *International Journal of Solids and Structures*, **41**, 1209-1234

9. Lagoudas D.C., Khan M.M., Mayes J.J., Henderson B.K., 2004, Pseudoelastic SMA spring element for passive vibration isolation: Part II – Simulation and experimental correlations, *Journal of Intelligent Material and Structure*, **15**, 443-470

10. Nayfeh A.H., Mook D.T., 1979, *Nonlinear Oscillations*, John Wiley and Sons, NY

11. Piccirillo V., Balthazar J.M., Pontes Jr. B.R., 2007a, Analytical study of the nonlinear behavior of a shape memory oscillator: Part I: Primary resonance and free response for low temperature, *Journal of Intelligent Material and Structure* (submitted)

12. Piccirillo V., Balthazar J.M., Pontes Jr. B.R., 2007b, Analytical study of the nonlinear behavior of a shape memory oscillator: Part II: Resonance secondary, *Journal of Intelligent Material and Structure* (submitted)

13. Piccirillo V., Balthazar J.M., Pontes Jr. B.R., Palacios J.L., 2007c, On nonlinear response of a non-ideal system with shape memory, *Proceeding of 9th Conference on Dynamical System Theory and Applications (DSTA-2007)*, Łódź, Poland

14. Savi M.A., Pacheco P.M.C.L., 2002, Chaos and hyperchaos in shape memory systems, *International Journal of Bifurcation and Chaos*, **12**, 645-657

15. Savi M.A., Pacheco P.M.C.L., Braga A.M.B., 2002, Chaos in a shape memory two-bars truss, *International Journal of Non-Linear Mechanics*, **37**, 1387-1395

16. Sommerfeld A., 1904, Naturwissenchftliche Ergebnisse der Neuren Technischen Mechanik, *Verein Deutscher Ingenieur Zeitscchrift*, **18**, 631-636

17. Tsuchida M., Guilherme K.L., Balthazar J.M., 2005, On chaotic vibrations of a non-ideal system with two degrees of freedom: 1:2 resonance and Sommerfeld effect, *Journal of Sound and Vibration*, **282**, 1201-1207

18. Warmiński J., Balthazar J.M., Brasil R.M.F.L.R.F., 2001, Vibrations of a non-ideal parametrically and self-excited model, *Journal Sound and Vibration*, **245**, 363-374

19. Wolf A., Swift J.B., Swinney H.L., Vastano J.A., 1985, Determining Lyapunov exponents from a time series, *Physica D*, **16**, 285-317

20. Zukovic M., Cveticanin L., 2007, Chaotic response in a stable Duffing system of non – ideal type, *Journal of Vibration and Control*, **13**, 751-767

O nieliniowym, chaotycznym i nieidealnym układzie drgającym z elementami wykazującymi efekt pamięci kształtu

Streszczenie

W pracy przedstawiono opis dynamiki nieliniowego układu złożonego z masy połączonej ze sztywnym podłożem za pośrednictwem elementu z pamięcią kształtu i tłumikiem. W celu realizacji wymuszenia w układzie zastosowano silnik prądu stałego z ograniczonym poborem mocy, który pobudza do ruchu masę, tworząc w ten sposób sprzężenie mechaniczne pomiędzy układem drgającym a źródłem energii. Element z pamięcią kształtu opisano za pomocą jednowymiarowego modelu fenomenologicznego opartego na teorii Devenshire'a. Przeanalizowano rozważany nieidealny układ opisany dwoma sprzężonymi nieliniowymi równaniami ruchu. Zaobserwowano i opisano interesujące zjawiska nieliniowe w postaci efektu Sommerfelda i nieliniowego rezonansu w zakresie drgań okresowych, chaotycznych i hiperchaotycznych.

Manuscript received November 19, 2007; accepted for print March 3, 2008